

# Vector magnetic hysteresis of hard superconductors

A. Badía<sup>1</sup> and C. López<sup>2</sup>

<sup>1</sup>*Departamento de Física de la Materia Condensada-I.C.M.A.,*

<sup>2</sup>*Departamento de Matemática Aplicada,*

*C.P.S.U.Z., María de Luna 3, E-50.015 Zaragoza (Spain)*

(October 29, 2018)

Critical state problems which incorporate more than one component for the magnetization vector of hard superconductors are investigated. The theory is based on the minimization of a cost functional  $\mathcal{C}[\vec{H}(\vec{x})]$  which weighs the changes of the magnetic field vector within the sample. We show that Bean's simplest prescription of choosing the correct sign for the critical current density  $J_c$  in one dimensional problems is just a particular case of finding the components of the vector  $\vec{J}_c$ .  $\vec{J}_c$  is determined by minimizing  $\mathcal{C}$  under the constraint  $\vec{J} \in \Delta(\vec{H}, \vec{x})$ , with  $\Delta$  a bounded set. Upon the selection of different sets  $\Delta$  we discuss existing crossed field measurements and predict new observable features. It is shown that a complex behavior in the magnetization curves may be controlled by a single external parameter, i.e.: the maximum value of the applied magnetic field  $H_m$ .

PACS number(s): 41.20.Gz, 74.60.Jg, 74.60.Ge, 02.30.Xx

## I. INTRODUCTION

The irreversible magnetization of type-II superconductors was successfully treated by Bean's critical state model (CSM) in the early sixties.<sup>1</sup> The basic idea is that the material develops a maximum (critical) current density in those regions which have been affected by an electric field, opposing to the magnetic flux changes. With remarkable simplicity, the CSM could explain the dependence of the magnetization on the macroscopic dimensions of the sample, as well as the observed hysteresis. Both features are a manifestation of the non-equilibrium thermodynamic processes which take place in the experiments and, thus, cannot be explained by the Abrikosov's flux line lattice (FLL) theory.<sup>2</sup> Furthermore, hard type-II materials develop such a pronounced hysteresis that the reversible contribution from the equilibrium FLL may be usually neglected. Nowadays, the hit of Bean's intuition is well understood in terms of the FLL dynamics in the presence of pinning centers.<sup>3</sup> In the process of punching vortices in or out the superconductor one produces metastable equilibrium states for which the gradient in the density of vortices is maximum. This results in the development of the macroscopic critical current density  $J_c$  and corresponds to the balance between a repulsive

vortex-vortex interaction and attractive forces towards the pinning centers.

Bean's *ansatz* has permitted the development of the theory with a maximum simplicity while incorporating the main experimental facts. However, it was early recognized insufficient for problems in which lattices of non-parallel flux tubes must be considered. For such cases, the current density within the sample is no more a vector with fixed direction, and additional prescriptions are required. On the other hand, a wealth of phenomena have been reported along the last decades associated to crossed field measurements. Refs. 4–7 provide some outstanding experiments, and the interested reader is directed to the papers cited therein for more complete landscape of the topic. Roughly speaking, when the experimental scenario is such that compression and rotation of vortices are induced, both the scalar repulsion between rigid parallel vortices and the cutting energy barrier for adjacent twisted flux lines come into play. In particular, this has consequences on the transport properties of type-II superconductors in a magnetic field, as the pinning of the FLL is strongly influenced by its internal stiffness.<sup>8</sup>

Several efforts have been made for the interpretation of rotating field experiments. Bean himself developed an approach for such problems.<sup>9</sup> However, to our knowledge, the most extensive general critical state theory is due to Clem and Pérez-González<sup>10–17</sup> who have developed the so-called double critical state model (DCSM). These authors have provided a physical basis for the limitations on the current flow both parallel and perpendicular to the local magnetic induction. Thus, the so-called parallel critical current density  $J_{c\parallel}$  and perpendicular critical current density  $J_{c\perp}$  were introduced.  $J_{c\parallel}$  relates to the flux cutting threshold, whereas  $J_{c\perp}$  stands for the *conventional* depinning current density. Recently, a more sophisticated approach was introduced, the so-called *two-velocity hydrodynamic model*.<sup>7</sup> Essentially, this theory incorporates the flux pinning and cutting phenomena within the framework of FLL's which consist of two vortex subsystems. Under certain circumstances it is fully equivalent to the DCSM, but, different, non-expected scenarios are also predicted.

In earlier work<sup>18,19</sup> we have envisioned the CSM realm as a phenomenological approach which can be formulated by means of a variational problem with constraints. This permits to deal with a wide class of restrictions on the current density. Thus, the optimal control (OC) theory<sup>20</sup> allows the minimization of a cost functional  $\mathcal{C}[\vec{H}(\vec{x})]$

which weighs the changes of the magnetic field vector within the sample under the constraint  $\vec{J} \in \Delta(\vec{H}, \vec{x})$ , with  $\Delta$  a bounded set. This general formulation gives freedom to fix the particular region  $\Delta$  of feasible current densities. For instance, the isotropic hypothesis  $|\vec{J}| \leq J_c$  corresponds to choosing  $\Delta$  as a disk, and the DCSM conditions  $|J_\perp| \leq J_{c\perp}$ ,  $|J_\parallel| \leq J_{c\parallel}$ , to an oriented rectangle.

In this work we present a detailed discussion of the variational principle (Sec.II), as well as the general aspects about the Hamiltonian equations which arise from our formulation (Sec. III). Sec.IV gathers a series of simulations of the field penetration profiles for two different selections of the control space  $\Delta$ . In particular, it is explicitly shown that the DCSM becomes a particular case of our treatment. Then, Sec. V is devoted to observe some properties of the magnetization loops which can be derived from the simulated profiles. In Sec.VI we give a general overview of the model and discuss the compatibility of different choices of  $\Delta$  with available experimental data.

## II. VARIATIONAL PRINCIPLE

In this section we will show that the coarse-grained electrodynamics of type-II superconductors in the critical state may be formulated as a minimization problem. From a more conventional side, on using the DCSM approach, one can obtain the successive field penetration profiles in a magnetization process by means of Maxwell differential equations, and the constitutive  $\vec{E}(\vec{J})$  law for the material. These equations, together with the boundary conditions allow to solve for the dependencies  $\vec{H}(\vec{x}, t)$ ,  $\vec{J}(\vec{x}, t)$ ,  $\vec{E}(\vec{x}, t)$ . As it is usual in hard superconductivity we are assuming  $\vec{B} = \mu_0 \vec{H}$ .

Now we recall that many physical theories, which are typically posed by a differential equation statement have been interpreted as the minimization of a given functional. For instance, the Lagrangian formulation of classical mechanics relies on the equivalence of Newton laws and the stationarity condition for the action  $S = \int L dt = \int (T - V) dt$ , when the time evolution of the system is determined. Below, we derive the functional  $\mathcal{C}$  whose minimization is equivalent to the standard approach for the critical state in superconductors. In order to gain physical insight, we will infer the CSM equations after considering some aspects of the more familiar eddy-current problem in normal metals ( $\vec{E} = \rho \vec{J}$ ). Assuming a discretization scheme in which  $\vec{H}_n$  stands for the magnetic field intensity at the time layer  $n\delta t$  and Ampère's law ( $\nabla \times \vec{H} = \vec{J}$ ), the successive field profiles in a magnetic diffusion process may be obtained by the finite-difference expression of Faraday's law

$$\mu_0 \frac{(\vec{H}_{n+1} - \vec{H}_n)}{\delta t} = -\nabla \times \vec{E} = -\rho \nabla \times (\nabla \times \vec{H}_{n+1}), \quad (1)$$

which defines a differential equation for  $\vec{H}_{n+1}$  in the spatial degrees of freedom. Then  $\vec{H}_{n+1}$  can be solved in terms of the previous field distribution  $\vec{H}_n$  and the boundary conditions at the time layer  $(n+1)\delta t$ . The minimization statement can be found by *inversion* of the Euler-Lagrange equations with respect to some Lagrange density that belongs to Eq.(1). The first term is straightforwardly inverted by integration with respect to the field  $\vec{H}_{n+1}$ . This gives  $\mu_0(H_{n+1}^2/2 - \vec{H}_n \cdot \vec{H}_{n+1})/\delta t$ , i.e.:

$$\frac{\partial(H_{n+1}^2/2 - \vec{H}_n \cdot \vec{H}_{n+1})}{\partial \vec{H}_{n+1}} = \vec{H}_{n+1} - \vec{H}_n.$$

The second term is a bit more involved as it cannot be transformed to an exact derivative with respect to the fields. However, if one introduces the notation  $(\nabla \times \vec{H}_{n+1})_i = \epsilon_{ijk} \partial_{x_j} H_{n+1,k}$  (with  $\epsilon_{ijk}$  the Levi-Civita tensor) it can be identified from

$$\partial_{x_j} \frac{\partial(\epsilon_{klm} \partial_{x_l} H_{n+1,m} \epsilon_{kpq} \partial_{x_p} H_{n+1,q})}{\partial(\partial_{x_j} H_{n+1,i})} = -2[\nabla \times (\nabla \times \vec{H}_{n+1})]_i.$$

Thus, Eq.(1) can be rewritten as:

$$\frac{\partial \mathcal{F}_{n+1}}{\partial H_{n+1,i}} - \partial_{x_j} \frac{\partial \mathcal{F}_{n+1}}{\partial(\partial_{x_j} H_{n+1,i})} = 0, \quad (2)$$

where

$$\mathcal{F}_{n+1} = \mu_0(H_{n+1}^2/2 - \vec{H}_n \cdot \vec{H}_{n+1}) + \rho \delta t (\nabla \times \vec{H}_{n+1}) \cdot (\nabla \times \vec{H}_{n+1})/2.$$

From variational calculus it is known that Eq.(2) corresponds to the necessary first order conditions for the functional  $\mathcal{C}_M = \int_\Omega \mathcal{F}_{n+1}$  to have a minimum with respect to the field  $\vec{H}_{n+1}$  (Euler-Lagrange equations).<sup>21</sup>

Finally, it is apparent that for minimization purposes  $\mathcal{C}_M$  may be completed by means of a constant term to the form

$$\mathcal{C}_M = \frac{\mu_0}{2} \int_\Omega |\vec{H}_{n+1} - \vec{H}_n|^2 + \frac{1}{2} \int_\Omega \rho \delta t (\nabla \times \vec{H}_{n+1}) \cdot (\nabla \times \vec{H}_{n+1}), \quad (3)$$

as  $\vec{H}_n(\vec{x})$  is considered to be given.

In conclusion, from the mathematical point of view, minimizing  $\mathcal{C}_M$  for each advancing time layer is just an equivalent statement of Faraday's laws in time discretized form. In addition, Eq.(3) allows a physical interpretation which can be used for comparison and generalization to other systems. Notice that the minimization of  $\mathcal{C}_M$  balances the *screening* term  $|\vec{H}_{n+1} - \vec{H}_n|^2$  and the *isothermal entropy production* term ( $\dot{S} = \vec{E} \cdot \vec{J}/T$ ). This can be identified as a quite general property of dynamical systems subjected to dissipative forces. The quasistationary time

evolution of the system holds a compensation between some *inertia* term and the irreversible loss of energy. The minimum principle for the global entropy production rate lies behind the previous statement. It was introduced by I. Prigogine<sup>22</sup> in the context of linear irreversible thermodynamics and applies for non-equilibrium stationary states. As a simple exercise, the reader can check that minimizing  $m|\vec{v}_{n+1} - \vec{v}_n|^2 + \gamma\vec{v}_{n+1} \cdot \vec{v}_{n+1}\delta t$  with respect to  $\vec{v}_{n+1}$  one reproduces the discretized statement of Newton's law for the motion of a particle against a viscous damping force. In the case of eddy currents  $|\vec{H}_{n+1} - \vec{H}_n|^2$  stands for the magnetic field inertia, including both the magnetostatic energy term  $\vec{H}_{n+1}^2$  and the term  $\vec{H}_n \cdot \vec{H}_{n+1}$ , which describes the work against electromotive forces.

Eventually, we notice that hard type-II superconductors may be treated by a modification of the functional  $C_M$  for normal metals. We want to emphasize that the concept of hard material is associated to a limiting case for the  $\vec{E}(\vec{J})$  characteristic, i.e: the electric field is zero for current densities below a critical value ( $J_c$ ) and abruptly raises to arbitrarily large values if  $J_c$  is overrun. In fact, this vertical graph limit is attained for the experimental situations in which the excitation typical period is large as compared to the magnetic diffusion time constant  $\tau_f \sim \mu_0 L^2 / \rho_f$ , where  $\rho_f$  stands for the flux flow resistivity and  $L$  is some typical length of the sample. Then, for current densities below  $J_c$ ,  $\vec{S}$  vanishes as no electric field is generated in stationary conditions. On the other side, in the approximation of arbitrarily large flux flow resistivity,  $\vec{S}$  would diverge if  $J > J_c$  and, thus,  $\mathcal{F}_{n+1}$  must be minimized constraining the current density to  $J \leq J_c$ . We wish to remark that the definition of critical current density may be done in a very general sense. In fact, one can postulate vertical  $\vec{E}(\vec{J})$  relations for definite directions of space as it is the case of the DCSM, in which one uses parallel and perpendicular projections with respect to the local magnetic field. One could even dictate that huge dissipation occurs whenever the current density vector  $\vec{J}$  lies outside some allowed region  $\Delta$ , generating an almost instantaneous change of the magnetic profile.

In the light of the previous discussion, the evolutionary critical state profiles can be obtained either by using Maxwell equations and a vertical  $\vec{E}(\vec{J})$  law or the principle:

*In a type-II superconducting sample  $\Omega$  with an initial field profile  $\vec{H}_n(\vec{x})$ , and under a small change of the external drive, the new profile  $\vec{H}_{n+1}$  minimizes the functional*

$$\mathcal{C}[\vec{H}_{n+1}(\vec{x})] = \frac{1}{2} \int_{\Omega} |\vec{H}_{n+1} - \vec{H}_n|^2, \quad (4)$$

*with the boundary conditions imposed by the external source, and the constraint  $\nabla \times \vec{H}_{n+1} \in \Delta(\vec{H}_{n+1}, \vec{x})$ .*

In this work we will concentrate on two particular cases which can be justified in terms of the underlying physical mechanisms. First, we will analyze the isotropic case

$|\vec{J}| \leq J_c$  (i.e.:  $\Delta$  is a disk). Then the variational formulation of the DCSM ( $J_{\parallel} \leq J_{c\parallel}, J_{\perp} \leq J_{c\perp}$ ) will be given. In this case  $\Delta$  is an oriented rectangle.

The next section is devoted to some aspects on the mathematical formalism of the optimal control theory. We will show that this method provides a very convenient framework for applying the variational principle stated above.

### III. HAMILTONIAN EQUATIONS

From the mathematical point of view, the problem of minimizing the action integral  $\mathcal{C}[\vec{H}_{n+1}(\vec{x})]$  [Eq.(4)] with  $\vec{H}_n(\vec{x})$  given, and  $\vec{H}_{n+1}$  fulfilling the differential equation

$$\nabla \times \vec{H}_{n+1} = \vec{J} \in \Delta \subset \mathbb{R}^3 \quad (5)$$

is a problem of variational calculus with nonholonomic constraints (constraints on the derivatives of the state variables). Being the constraint set  $\Delta$  a compact region with boundary, we must take into account the possibility that the minimum is either reached in an interior point or in a boundary point. The machinery generalizing the classical variational calculus to sets with boundaries is the maximum principle of optimal control, introduced by Pontryagin.<sup>20</sup> OC is a standard theory in engineering, where dynamical systems are actuated by external controls (limited to some maximal values) in order to get a desired behaviour. The given system of differential equations, including the effect of external actions is named the control system, and the integrand of the minimizing functional is the cost or performance function. The mathematical problem here is similar, with Ampere's law as control system and performance function  $\frac{1}{2}|\vec{H}_{n+1} - \vec{H}_n|^2$ , although of course the bounded variable  $\vec{J}$  is not an external control. As we will see later on, the algebraic condition of maximality embraces the cases of interior and boundary optimal points, therefore including the classical equations of variational calculus for unconstrained problems, and the modified equations for minimal solutions in the boundary. In addition to the original reference,<sup>20</sup> the interested reader is invited to review Refs. 23,24 for a more comprehensive and topical statement of the OC machinery.

In this paper, in order to simplify the presentation, we fix the geometry of the sample to be an infinite slab, so that the control system (Ampere's law) becomes by symmetry considerations a simple system of ordinary differential equations. Other geometries, as the cylinder, give way to different control systems, and the case of a finite sample generates a more involved system of partial differential equations. For the slab geometry, with applied magnetic field parallel to the faces we have

$$\frac{d\vec{H}_{n+1}}{dx} = \vec{f}(\vec{H}_{n+1}, \vec{u}, x) \quad \vec{f} \in \Delta$$

as control system. Hereafter, we take the X axis perpendicular to the slab faces and the origin of coordinates at the midplane. By construction, the vector  $\vec{f} = (0, f_y, f_z)$  is orthogonal to the physical variable  $\vec{J}$ ,  $f_y = J_z$ ,  $f_z = -J_y$ . Notice that, despite the applied rotation, we use the same notation for the allowed control set  $\Delta$ . Note also that the function  $\vec{f}$  has dependence on the local magnetic field (this allows to include the usual models  $J_c(|\vec{H}|)$ , and possible anisotropy), on the position (for potentially inhomogeneous materials) and on some independent coordinates  $\vec{u}$ , the control variables in OC notation, parameterizing the region  $\Delta$ .

The first step in the theory of constrained variational calculus is the definition of a Hamiltonian density, containing the performance function, and momenta variables that play the role of Lagrange multipliers for the constraints.

$$\mathcal{H}(\vec{H}_{n+1}, \vec{u}, \vec{p}, x) \equiv \vec{p} \cdot \vec{f} - \frac{1}{2} |\vec{H}_{n+1} - \vec{H}_n(x)|^2. \quad (6)$$

Recall that here  $\vec{H}_n(x)$  is a given profile. It is important to notice that  $\mathcal{H}$  is not the usual Hamiltonian function of Classical Mechanics in phase space; here it depends on the usual state  $\vec{H}_{n+1}$  and momenta  $\vec{p}$  variables, but additionally on the control  $\vec{u}$ . Therefore, the associated equations are not only the Hamiltonian differential equations but also an extra algebraic condition of maximality, in order to determine the extra variables  $\vec{u}$ . Denoting by  $\vec{H}_{n+1}^*(x)$ ,  $\vec{p}^*(x)$  and  $\vec{u}^*(x)$  the optimal solution functions (i.e. minimizing  $\mathcal{C}$  and satisfying the control system), the OC equations are

$$\frac{d\vec{H}_{n+1}^*}{dx} = \frac{\partial \mathcal{H}}{\partial \vec{p}} = \vec{f}(\vec{H}_{n+1}^*, \vec{u}^*, x), \quad (7)$$

the adjoint equations for the momenta

$$\frac{d\vec{p}^*}{dx} = -\frac{\partial \mathcal{H}}{\partial \vec{H}_{n+1}} = \vec{H}_{n+1}^* - \vec{H}_n(x) - \vec{p}^* \cdot \frac{\partial \vec{f}}{\partial \vec{H}_{n+1}}(\vec{H}_{n+1}^*, \vec{u}^*, x), \quad (8)$$

and the algebraic condition of maximality

$$\mathcal{H}(\vec{H}, \vec{u}^*, \vec{p}, x) \geq \mathcal{H}(\vec{H}, \vec{u}, \vec{p}, x) \quad \forall \vec{f}(\vec{H}, \vec{u}, x) \in \Delta. \quad (9)$$

$\vec{H}$  and  $\vec{p}$  are fixed in this last condition. In general, this allows to find a relation  $\vec{u}^*(\vec{H}, \vec{p}, x)$ . When this relation is replaced in the former Hamiltonian equations [Eqs.(7) and (8)], a well posed system of ordinary differential equations appears.

For the class of Hamiltonian  $\mathcal{H}$  described above, the algebraic condition of maximality is fulfilled for a vector  $\vec{f}$  with maximum projection over the momentum  $\vec{p}$ . As a simple exercise, the reader is invited to check that this rule produces the Bean CSM for one dimensional problems (parallel vortices). Thus, on choosing  $\vec{H} = H_z \hat{z}$

one has  $f = -J_y$ . The restriction on the current density reads  $J_y = uJ_c$  with  $|u| \leq 1$ . Then, Eq.(9) gives  $u^* = \text{sgn}(p)$  and this leads to  $f = \pm J_c$  in agreement with Bean's prescription. Remarkably, for the case of multidimensional systems (non-parallel vortices) the maximality condition will give the *critical current* vector both in modulus and direction. Note that  $\vec{J}$  is determined dynamically, through the evolution of the momentum vector. The specific details on the distribution rule for the components of  $\vec{J}_c$  depend on the control space  $\Delta$  and will be discussed in the next section.

As regards the boundary conditions that must be used for obtaining the solution profiles  $\vec{H}_{n+1}^*(x)$  from Eqs.(7) and (8), several considerations must be made. Firstly, in the absence of demagnetizing effects,  $\vec{H}_{n+1}^*$  is determined on the faces of the slab by continuity of the external applied field. For the remaining boundary conditions, two typical situations appear. In the first case, the modified penetrating profile  $\vec{H}_{n+1}^*(x)$  equals the former profile  $\vec{H}_n(x)$  before reaching the centre of the slab. This gives place to an (unknown in advance) point  $x^*$  such that  $\vec{H}_{n+1}^*(x) = \vec{H}_n(x) \quad \forall x \leq x^*$ . The free boundary condition  $\mathcal{H}(x^*) = 0$  applies in this case, and allows to determine  $x^*$ . In the second case, the new profile never meets the former one, and the value of  $\vec{H}_{n+1}^*(0)$  is unknown; then, the corresponding transversality condition  $\vec{p}^*(0) = \mathbf{0}$  completes then the number of required boundary conditions.

#### IV. FIELD PENETRATION PROFILES

The Hamiltonian formalism developed above can be expeditiously applied to calculate the field penetration profiles for magnetization processes in which non-parallel vortex configurations are enforced. As the applied field is assumed to be the same on both sides of the slab under consideration, we can restrict to the interval  $0 \leq x \leq a$ . By virtue of the symmetry, the same behavior appears for  $-a \leq x \leq 0$ .

##### A. Isotropic model

First, we will derive some results for the field penetration process in the so-called isotropic hypothesis:  $|\vec{J}| \leq J_c$ . In order to show the capabilities of the model, a field dependence  $J_c(H)$  will be allowed. In particular, the Kim's model<sup>25</sup> expression  $J_c(H) = J_{c0}/(1 + H/H_0)$  will be used. Recall that the microstructure dependent parameters  $J_{c0}, H_0$  are included. For convenience, the following dimensionless units are introduced:  $x$  is given in units of  $a$ ,  $H$  in units of  $H_0$ , and  $J$  in units of  $H_0/a$ . Then, the statement of Ampère's law, together with the critical current restriction read

$$\frac{d\vec{H}_{n+1}}{dx} = \vec{f}(\vec{H}_{n+1}, \vec{u}, x) = \frac{\beta \vec{u}}{1 + |\vec{H}_{n+1}|} \quad |\vec{u}| \leq 1.$$

Above we have introduced the dimensionless constant  $\beta = J_c a / H_0$  and the so-called *control variable*  $\vec{u}$ , which is a vector within the unit disk  $D$ . This means that the current density belongs to a disk of variable radius, depending on the local magnetic field. Thus, following the OC terminology, we have the *control equations* for the *state variables*  $\vec{H}_{n+1}(x)$ .

Next, we require the minimization of the *functional*  $\mathcal{C}[\vec{H}_{n+1}(x)]$  constrained by the state equations. Following the OC machinery introduced in Sec.III, the maximization of the associated Hamiltonian  $\mathcal{H}$  [Eq.(6)] with respect to the control variable  $\vec{u}$  leads to the condition  $\vec{u}^* = \vec{p}^* / p^*$ . This has the physical counterpart  $|\vec{J}| = J_c(H)$ , i.e.: within the isotropic model, the maximum allowed current density modulus  $J_c$  is carried within those regions which have been affected by the perturbation. Then, the Hamiltonian equations that provide the field profile are

$$\frac{dH_{n+1,i}^*}{dx} = \frac{p_i^*}{p^*} \frac{\beta}{1 + H_{n+1}^*} \quad (10a)$$

$$\frac{dp_i^*}{dx} = H_{n+1,i}^* - H_{n,i} + \frac{\beta p^* H_{n+1,i}^*}{H_{n+1}^* (1 + H_{n+1}^*)^2}. \quad (10b)$$

Eventually, appropriate boundary conditions must be supplied to solve this set of equations. As it was discussed in Sec.III these conditions are given by the external drive values, together with the field penetration regime. If the new profile matches the old one at a point  $0 < x^* < 1$  (partial penetration) one uses  $\vec{H}_{n+1}^*(x^*) = \vec{H}_n(x^*)$  and  $\mathcal{H}(x^*) = 0$ . Within the full penetration regime, however, one uses the momenta transversality conditions  $\vec{p}^*(0) = \mathbf{0}$ .

In order to illustrate the bundle of phenomena which can be expected in crossed field measurements, we have calculated the penetration profiles for a zero field cooled sample to which a constant excitation  $H_{zS}$  is applied, followed by cycling stages of the other field component at the surface  $H_{yS}$ . We want to emphasize that, in order to approximate the continuum evolution, small increments of  $H_{yS}$  have been applied in the iterative solution of Eqs.(10a) and (10b). However, for clarity, only a selection of representative field and current density curves are depicted. The value of  $\beta$  is set to unity for definiteness hereafter.

### 1. Initial magnetization process

Fig.1 displays the penetration profiles for the initial magnetization process that is induced by increasing the surface field  $H_{yS}$ . We notice that the conventional  $H_z(x)$  profile (which was obtained by the standard CSM) is

pushed towards the center as  $H_{yS}$  increases. In physical terms, a current flow  $J_z$  is required for shielding the new field component  $H_y$ . Owing to the constraint  $|\vec{J}| = J_c(H)$ , this results in a reduction of  $J_y$  (the slope of  $H_z$ ) and  $H_z$  develops a subcritical behavior. Just for clarity, we have only plotted advancing fronts until the centre of the sample is reached. Ongoing profiles will be shown in the next subsections.

### 2. Low field hysteresis

Here, we analyze the hysteresis effects which can be observed when the surface field is cycled. First, the maximum applied field ( $-H_m \leq H_{yS} \leq H_m$ ) is chosen so as to keep a zero field value at the midplane. We define the penetration field  $H_m^*$  as the value of  $H_{yS}$  for which the front reaches the point  $x = 0$ . This is somehow equivalent to the so-called partial penetration regime in the standard CSM. However, notice that now  $H_m^*$  depends on the previously set value of  $H_{zS}$ . Fig.2 displays the results. It can be observed that  $H_y(x)$  basically shows a conventional critical state behavior, whereas  $H_z(x)$  develops a prominence. This shape relates to the corresponding slope reduction near the surface ( $x = 1$ ) and the subsequent reentry in the unperturbed profile. Physically, the distribution rule for the current density vector enhances the  $J_z$  component near the surface in order to shield the change in  $H_y$  (i.e.: reducing  $\int |\vec{H}_{n+1} - \vec{H}_n|^2 dx$ ). Then,  $J_y$  diminishes and, therefore  $H_z(x)$  flattens. An internal slope increase is obviously required for the previous profile  $H_{n,z}(x)$  to be reached at some point  $0 < x^* < 1$ . Notice the *peak structure* that appears in  $J_y(x)$  and the corresponding sign change in the  $J_z$  component. The point of vanishing  $J_z$  determines the maximum of the peak structure in  $J_y$ , i.e.: the full current flow is parallel to the Y axis.

### 3. Intermediate field hysteresis

When the maximum applied field  $H_m$  is allowed to increase beyond  $H_m^*$  new phenomena appear. Fig.3 displays some outstanding features, which are sketched here: (i) it is apparent that the  $H_y(x)$  curves do not show a conventional hysteresis cycle structure. Notice that the profiles no.1 and no.11 that correspond to  $H_{yS} = H_m$  do not fit. (ii) Contrary to the case of low field cycles, the profiles  $H_z(x)$  do not repeat values for the ascending/descending branches. When the sample centre is reached (profile no.4) irreversible flux entry happens (no.5 and no.6). Further changes (curves no.7 to no.11) occur over a reduced shielding curve. Finally, one can see that the aforementioned features are clearly translated to the current density vector  $\vec{J}(x)$ .

#### 4. High field hysteresis

In this part we show that, within the isotropic model, a transverse field  $H_{yS}$  may effectively collapse the longitudinal diamagnetic profile  $H_z(x)$ . Fig.4 displays a magnetization process in which  $H_{yS}$  is increased up to the value  $H_m = 3$  in our dimensionless units. Then,  $H_{yS}$  is decreased down to  $H_m = -3$ . Further increase to  $H_m = 3$  is not shown just to avoid intricacy in the graph. However, the complete hysteresis cycle will be presented in the next section. Here one can see that  $H_y(x)$  follows a typical CSM high field evolution, whereas  $H_z(x)$  irreversibly evolves to a flat profile, compatible with the boundary condition  $H_z(1) = H_{zS}$ . Simultaneously, the current density related to  $H_z$  becomes zero. Thus, a constant trapped field  $H_{zS}$  is generated within the sample. Any subsequent change in  $H_{yS}$  will not affect the trapped field and the associated current density component.

The described behavior can be well understood in terms of the minimization principle. The process tends to minimize

$$\mathcal{C} = \frac{1}{2} \int_{\Omega} (H_{n+1,y} - H_{n,y})^2 + (H_{n+1,z} - H_{n,z})^2 .$$

It is apparent that if the condition  $H_{n+1,z}(x) = H_{n,z}(x)$  is fulfilled,  $\mathcal{C}$  cannot be smaller than the minimum value of  $1/2 \int (H_{n+1,y} - H_{n,y})^2$ , which appears for the full current flow dedicated to  $H_y$ . Thus, one has  $J_z = \pm J_c$  and  $J_y = 0$ , and both conditions hold thereafter.

#### B. Double critical state model

Below we will show that our approach reproduces the results derived by the standard DCSM when the appropriate control space for the current density is chosen. For this purpose we focus on Ref. 12 in which the DCSM was used for investigating a wealth of phenomena in rotating field experiments. In order to ease comparison, we shall adopt the notation therein. An infinite slab with surfaces at  $x = 0$  and  $x = 2X_m$  was considered with the magnetic field contained in the YZ plane.

The starting point will be the restatement of the functional  $\mathcal{C}$  in appropriate generalized coordinates

$$\mathcal{C}[\vec{H}_{n+1}(\vec{x})] = \frac{1}{2} \int_{\Omega} H_{n+1}^2 - 2H_n H_{n+1} \cos(\alpha_{n+1} - \alpha_n) .$$

Here  $H, \alpha$  stand for the field modulus and the angle with respect to the Y axis.  $H_n, \alpha_n$  correspond to the given previous profile and one must solve for  $H_{n+1}, \alpha_{n+1}$ . Now,  $\mathcal{C}$  must be minimized with the constraints

$$\left| \frac{dH_{n+1}}{dx} \right| \leq J_{c\perp} \quad ; \quad \left| \frac{d\alpha_{n+1}}{dx} \right| \leq k_{c\parallel} ,$$

where  $J_{c\perp}$  and  $k_{c\parallel}$  are the constants characterizing the flux pinning and cutting thresholds. Following Ref. 12

$k_{c\parallel}$  relates to the parallel critical current density by  $k_{c\parallel} = J_{c\parallel}/H$ .

On defining the characteristic length scale  $\lambda \equiv 1/k_{c\parallel}$ , and using  $H$  in units of  $J_{c\perp}\lambda$  and  $x$  in units of  $\lambda$ , one obtains the dimensionless expressions

$$\frac{dH_{n+1}}{dx} = \frac{J_{\perp}}{J_{c\perp}} \equiv u_h \quad ; \quad |u_h| \leq 1$$

$$\frac{d\alpha_{n+1}}{dx} = \frac{k_{\parallel}}{k_{c\parallel}} \equiv u_{\alpha} \quad ; \quad |u_{\alpha}| \leq 1$$

In other words, the control set  $\Delta$  is a square in this units.

Next, we introduce the associated Hamiltonian [Eq.(6) in Sec.III]

$$\mathcal{H} = p_h u_h + p_{\alpha} u_{\alpha} - \frac{1}{2} [H_{n+1}^2 - 2H_n H_{n+1} \cos(\alpha_{n+1} - \alpha_n)] .$$

Then, if one applies the Pontryagin's maximum principle

$$\max_{\vec{u} \in \Delta} \mathcal{H} \equiv \max_{\vec{u} \in \Delta} (p_h u_h + p_{\alpha} u_{\alpha})$$

$(u_h^*, u_{\alpha}^*)$  is determined again as a vector leaning on the boundary of  $\Delta$ . This has been illustrated in Fig.5 and relies on the fact that  $\vec{p} \cdot \vec{u}$  is maximum for the largest projection of  $\vec{u}$  on  $\vec{p}$ . If  $(p_h, p_{\alpha})$  are non-vanishing, one gets  $(u_h^*, u_{\alpha}^*) = [\text{sgn}(p_h), \text{sgn}(p_{\alpha})]$ , which can be identified as a CT-zone within the DCSM framework. On the other hand,  $p_h \neq 0, p_{\alpha} = 0$  in an open interval will give place to a T-zone in which  $u_h^* = \text{sgn}(p_h)$  and  $u_{\alpha}^*$  must be determined on the basis of other arguments. Finally,  $p_h = 0, p_{\alpha} \neq 0$  corresponds to a C-zone, in which  $u_{\alpha}^* = \text{sgn}(p_{\alpha})$  and  $u_h^*$  is yet undetermined.

Thus, in the case under consideration (i.e.: field independent  $J_{c\perp}, k_{c\parallel}$ ) the Hamiltonian equations are

$$\frac{dH_{n+1}}{dx} = \text{sgn}(p_h) \quad \text{or} \quad \text{undetermined} \quad (11a)$$

$$\frac{d\alpha_{n+1}}{dx} = \text{sgn}(p_{\alpha}) \quad \text{or} \quad \text{undetermined} \quad (11b)$$

$$\frac{dp_h}{dx} = H_{n+1} - H_n \cos(\alpha_{n+1} - \alpha_n) \quad (11c)$$

$$\frac{dp_{\alpha}}{dx} = H_{n+1} H_n \sin(\alpha_{n+1} - \alpha_n). \quad (11d)$$

These equations can be straightforwardly solved to produce the field penetration profiles. Different expressions arise related to the mentioned zone structure.

##### 1. CT zone

If one has  $p_h \neq 0, p_{\alpha} \neq 0$ , the field penetration is given by the differential equations

$$\frac{dH_{n+1}}{dx} = \text{sgn}(p_h) \quad \Rightarrow \quad H_{n+1} = \text{sgn}(p_h)x + H_{n+1}(0)$$

$$\frac{d\alpha_{n+1}}{dx} = \text{sgn}(p_{\alpha}) \quad \Rightarrow \quad \alpha_{n+1} = \text{sgn}(p_{\alpha})x + \alpha_{n+1}(0) .$$

Above, we have incorporated surface boundary conditions, just for definiteness.

### 2. T zone

In this case one has

$$H_{n+1} = \text{sgn}(p_h)x + H_{n+1}(0)$$

and  $\alpha_{n+1}(x)$  is determined by the condition  $dp_\alpha/dx = 0$ , which guarantees that  $p_\alpha$  keeps the zero value in this region. Then

$$H_{n+1}(x)H_n(x) \sin[\alpha_{n+1}(x) - \alpha_n(x)] = 0$$

### 3. C zone

In this case one has

$$\alpha_{n+1} = \text{sgn}(p_h)x + \alpha_{n+1}(0)$$

and  $H_{n+1}(x)$  is determined by the condition  $dp_h/dx = 0$ , which gives

$$H_{n+1}(x) = H_n(x) \cos[\alpha_{n+1}(x) - \alpha_n(x)]$$

### 4. Example: nonmagnetic initial state

Several initial magnetic configurations were examined in Ref. 12 within the conventional DCSM formulation. For illustration, the nonmagnetic initial state, which corresponds to the so-called field cooled experiment is analyzed here in the framework of our theory.

We assume initial uniform flux density within the superconductor  $H_0(x) = H_s, \alpha_0(x) = 0$ . Then, consider the quasisteady evolution towards the state  $H_{n+1}(x), \alpha_{n+1}(x)$  with boundary conditions at the surface  $H_{n+1}(0) = H_s$  and  $\alpha_{n+1}(0) = (n+1)\delta\alpha \equiv \alpha_{s,n+1}$ . The minimization of  $\mathcal{C}$  for the  $n+1$  time layer requires an initial CT-zone given by

$$\begin{aligned} H_{n+1}(x) &= H_s - x \quad ; \quad p_h < 0 \\ \alpha_{n+1}(x) &= \alpha_{s,n+1} - x \quad ; \quad p_\alpha < 0 . \end{aligned}$$

The CT-zone spreads up to the point  $x_{v,n+1}$  where the conditions  $p_h = 0, dp_h/dx = 0$  are reached. This point may be determined by iteration of the governing Hamiltonian equations (Eqs. (11)) over the previous steps. Such process leads to

$$\begin{aligned} H_s - x_{v,n+1} - H_n(x_{v,n+1}) \cos(\delta\alpha) &= 0 \quad \Rightarrow \\ x_{v,n+1} &= H_s [1 - \cos(\alpha_{s,n+1} - x_{v,n+1})] \end{aligned}$$

and defines the beginning of a C-zone. The equation determining  $x_{v,n+1}$  has been obtained within the approximation  $\delta\alpha \rightarrow 0 \Rightarrow \cos^n(\delta\alpha) \rightarrow 1$ . This condition yields the continuum limit of our discretized approach. Notice that our expression matches the one obtained by the conventional DCSM. Finally, the C-zone stretches from  $x_{v,n+1}$  to  $x_{c,n+1}$ , the point where  $\alpha_{n+1}$  vanishes. Then, the field modulus profile becomes

$$H_{n+1}(x) = H_s \cos(\alpha_{s,n+1} - x) . \quad (12)$$

The associated momenta  $p_h, p_\alpha$  may be straightforwardly obtained by integration of their first order differential equations. In Fig.6 we have plotted the first step profiles  $H_1(x), \alpha_1(x), p_h(x), p_\alpha(x)$ . Several points have been marked on the curves  $p_h(x)$  and  $p_\alpha(x)$ , that correspond to the sequence of values of the control variable  $\vec{u}$  standing out in Fig.5. Notice that  $(u_h, u_\alpha)$  always takes values on the boundary of the control space. Within a CT-zone  $\vec{u}$  remains on a vertex of the square. As soon as a component of  $\vec{p}$  vanishes (point 3 in our example) the associated component of  $\vec{u}$  must be determined by the condition of zero derivative. In our case, this produces a jump to the vector  $\vec{u}_3$ , which defines the beginning of the C-zone ( $\vec{u}_3, \vec{u}_4, \vec{u}_5, \dots$ ). This jump in the control variable is known as *bang-bang* phenomenon among mathematicians. Eventually, if the center of the sample is not reached by the variations, a new jump in the current density gives way to the O-zone ( $u_h = 0, u_\alpha = 0$ ).

## V. MAGNETIZATION LOOPS

Though some experiments have been devised for the direct measurement of the field or current penetration profiles, the common practice is to record average values. Thus, the vast majority of data on vortex matter in type II superconductors consist of magnetic moment measurements. Recall that the macroscopic magnetization of the sample is defined as  $\vec{M} \equiv \langle \vec{H}(x) \rangle - \vec{H}_S$ , where  $\vec{H}_S$  stands for the uniform applied field.

In this section we concentrate on the magnetization loops which can be derived from the previously treated field penetration profiles. It will be shown that important experimental results can be reproduced. New observable features are also predicted, which may be used as a test for the physically meaningful critical current control space. All the results presented below correspond to the isotropic hypothesis, which has been mainly developed in this paper. The comparison to the already well established DCSM and a discussion on the selection of the control space for the current density are considered in the next section.

First, we analyze the influence of the maximum applied field  $H_m$  on the magnetization loop. Fig.7 collects the results corresponding to the profiles analyzed in SubSec.IV A: low field ( $H_m < H_m^*$ ), intermediate field ( $H_m > H_m^*$ ), and high field ( $H_m \gg H_m^*$ ). We have

depicted both  $M_y$  and  $M_z$  for the zero field cooled process: (i) Apply  $H_{zS}$ , (ii) increase  $H_{yS}$  from zero to  $H_m$ , (iii) decrease  $H_{yS}$  to  $-H_m$ , and (iv) increase  $H_{yS}$  to  $H_m$  again.

$M_y(H_{yS})$  roughly displays a standard behavior, but shows a noticeable peculiarity for the intermediate field loop. The loop fails to close after a complete field cycle. This feature was not noticed for the low/high field loops, at least to the numerical precision of our calculations. The  $M_z(H_{yS})$  curves show a quite less conventional behavior as compared to one dimensional measurements in which a single field component appears. In addition, qualitatively different tendencies can be observed in terms of the value  $H_m$ . Thus, low field cycles produce a *butterfly* loop; intermediate fields produce a descending behavior for the transverse magnetic moment, and high fields produce the irreversible collapse of magnetization.

As a final observation, we describe an outstanding feature that was observed in our simulations. A second cycle in the applied field  $H_{yS}$  succeeds to close the hysteresis loop  $M_y(H_{yS})$  in the intermediate field region. Meanwhile,  $M_z$  keeps the descending trend, though seeming to stabilize around a non-vanishing value. This has been depicted in Fig.8.

We want to emphasize that our intermediate field simulations reproduce the experimental observations in Ref. 5 and in some related papers cited therein. Thus, the isotropic hypothesis sets a simple model for those crossed field measurements. Furthermore, we suggest to extend such measurements as a test of the theory, i.e.: perform low/high field loops and a second cycle in order to check the predicted features.

## VI. DISCUSSION AND CONCLUSIONS

We have introduced a variational formulation that generalizes Bean's critical state model for hard superconductors, while keeping its conceptual simplicity. In the spirit of the original theory, we have also avoided the explicit use of the electric field  $\vec{E}$ . However, the time evolution of the magnetic field profiles  $\vec{H}(x, t)$  can be obtained by replacing  $\vec{E}$  with an appropriate restriction on the current density  $\vec{J}$  flowing within the sample. Mathematically, a wide range of possibilities are allowed as we pose it in the form  $\vec{J} \in \Delta(\vec{H}, x)$  with  $\Delta$  a bounded set. Upon the selection of a definite set  $\Delta$ , our theory may be considered as the background for a variety of critical state models. In particular, we have analyzed the cases of choosing either a circle or a rectangle (isotropic model and DCSM respectively).

The variational quantity which is minimized under the aforementioned restriction has got a clear physical interpretation and quite general validity. We propose that the time evolution is governed by the balance between a screening term (inertia) and an entropy production term. This relies on basic principles of non-equilibrium

thermodynamics.<sup>22</sup> Within the usual assumption of instant response (vertical  $\vec{E}(\vec{J})$  graph) the singular behavior of  $\dot{S} = \vec{E} \cdot \vec{J}/T$  is treated by replacing the associated term with the condition  $\vec{J} \in \Delta$  in the minimization principle. This kind of statement fits the mathematical theory of optimal control,<sup>20</sup> that has been applied in this paper. The method is appropriate for the numerical treatment of realistic problems in which the magnetization is a vector quantity. Such situation occurs in experimental setups designed for studying the interaction of twisted vortices and in the field of technological applications of hard type-II superconductors.

We want to emphasize that the selection of the permitted set  $\Delta$  for the current density should be either justified in terms of fundamental theories or bounded by experimental observations. The scope of our paper is to provide a suitable mathematical treatment for general CSM problems and a physical background for the method. A well posed inversion theory, allowing to obtain the set  $\Delta$  from experiments is still an open question.

However, some conclusions can be drawn from the comparison of simulations with different sets  $\Delta$ . On the one side, some experimental observations are quite independent of the region  $\Delta$  in use. This is the case of the field penetration profiles in rotating field experiments. A very similar behavior is predicted either by the isotropic or DCSM hypothesis.<sup>19</sup> On the other side, one can find outstanding differences between these two models. Firstly, the former predicts the criticality condition  $J = J_c$  for those regions which have been affected by an electric field. Within the DCSM framework, however, one can obtain *critical* regions (CT zones) where  $J = J_c = \sqrt{(J_{c\parallel}^2 + J_{c\perp}^2)}$  and *subcritical* regions (C or T zones) where  $J < J_c$ . Microscopic probes can be used to investigate this property. For instance, Ref. 26 reports neutron polarization analysis of the magnetic field profiles within ceramic YBCO samples subjected to rotation stages. The isotropic hypothesis seems to be favoured for this Josephson medium. On the macroscopic side, one can design adequate experiments which check the compatibility with specific selections of  $\Delta$ . The investigation of the so-called *magnetization collapse*<sup>7</sup> is a promising possibility. In fact, recent experimental results on melt-textured and single crystal YBCO samples<sup>27,28</sup> are nicely described within the isotropic model. The authors of Ref. 28 have studied the transverse magnetic moment  $M_z$  suppression by cycling the longitudinal magnetic field  $H_{yS}$ . As the most important observed feature they emphasize the symmetric decrease of  $M_z$  for the diamagnetic and paramagnetic initial states of the sample. This is shown to be in clear contradiction with the DCSM hypothesis and qualitatively interpreted by their *two-velocity hydrodynamic model*. In Fig.9 we show that our general critical state theory gives a quite satisfactory explanation of the experimental facts. We get a symmetric suppression of  $M_z$ . The field penetration profiles show that the slope decrease in  $H_z(x)$  near the surface, due to the enhance-

ment of the current density component which shields the change in  $H_y$ , occurs in a quite similar fashion, regardless the initial magnetic state. Additionally, we want to notice that the behavior of  $M_z$  upon a second cycle in  $H_{yS}$  which is observed in our simulations (see Fig.8) gives further evidence of the validity of the model. The coincidence with the experimental data depicted in Fig.5 of Ref. 28 is remarkable.

Finally, we will comment on some future extensions of our work. Here we have used a time-discretization scheme, and a slab geometry, in order to produce an ordinary differential equation statement of our principle. This simplifies the theory, but should not be considered as a limitation. Optimal control for systems governed by partial differential equations may be applied for more general cases. Thus, one could afford a continuum approach to the problem and also include the sample finite size effects if necessary. Other issues as the use of different physically meaningful control sets  $\Delta$  (f.i.: elliptic, so as to incorporate material anisotropy), spatial inhomogeneity or surface barrier effects are also suggested.

#### ACKNOWLEDGEMENTS

The authors acknowledge financial support from Spanish CICYT (projects MAT99-1028 and BFM-2000-1066/C0301).

- 
- <sup>1</sup> C. P. Bean, Phys. Rev. Lett. **8**, 250 (1962); Rev. Mod. Phys. **36**, 31 (1964).  
<sup>2</sup> A. A. Abrikosov, Zh. Eksperim. i Teor. Fiz. **32**, 1442 (1957) [Sov. Phys.-JETP **5**, 1174 (1957)].  
<sup>3</sup> R. A. Richardson, O. Pla, and F. Nori, Phys. Rev. Lett. **72**, 1268 (1994).  
<sup>4</sup> J. R. Cave and M. A. R. LeBlanc, J. Appl. Phys. **53**, 1631 (1982).  
<sup>5</sup> S. J. Park, J. S. Kouvel, H. B. Radousky, and J. Z. Liu, Phys. Rev. B **48**, 13998 (1993).  
<sup>6</sup> M. A. R. LeBlanc, S. Celebi, S. X. Wang, V. Plecháček, Phys. Rev. Lett. **71**, 3367 (1993).  
<sup>7</sup> I. F. Voloshin, A. V. Kalinov, S. E. Savel'ev, L. M. Fisher, V. A. Yampolskiĭ, and F. Pérez-Rodríguez, JETP **84**, 592 (1997).  
<sup>8</sup> A. Sudbø and E. H. Brandt, Phys. Rev. Lett. **67**, 3176 (1991).  
<sup>9</sup> C. P. Bean, J. Appl. Phys. **41**, 2482 (1970).  
<sup>10</sup> J. R. Clem, Phys. Rev. B **26**, 2463 (1982).  
<sup>11</sup> J. R. Clem and A. Pérez-González, Phys. Rev. B **30**, 5041 (1984).  
<sup>12</sup> A. Pérez-González and J. R. Clem, Phys. Rev. B **31**, 7048 (1985).  
<sup>13</sup> A. Pérez-González and J. R. Clem, J. Appl. Phys. **58**, 4326 (1985).

- <sup>14</sup> A. Pérez-González and J. R. Clem, Phys. Rev. B **32**, 2909 (1985).  
<sup>15</sup> J. R. Clem and A. Pérez-González, Phys. Rev. B **33**, 1601 (1986).  
<sup>16</sup> A. Pérez-González and J. R. Clem, Phys. Rev. B **43**, 7792 (1991).  
<sup>17</sup> F. Pérez-Rodríguez, A. Pérez-González, J. R. Clem, G. Gandolfini, M. A. R. LeBlanc, Phys. Rev. B **56**, 3473 (1997).  
<sup>18</sup> A. Badía, C. López, and J. L. Giordano, Phys. Rev. B **58**, 9440 (1998).  
<sup>19</sup> A. Badía and C. López, Phys. Rev. Lett. **87**, 127004 (2001).  
<sup>20</sup> L. S. Pontryagin, V. Boltyanskiĭ, R. Gramkrelidze, and E. Mischenko, *The Mathematical Theory of Optimal Processes* (Wiley Interscience, New York, 1962).  
<sup>21</sup> G. Arfken and H. J. Weber, *Mathematical Methods for Physicists* (Academic, Boston, 1995), 4th ed.  
<sup>22</sup> I. Prigogine, *Introduction to Thermodynamics of Irreversible Processes* (North-Holland, Amsterdam, 1967).  
<sup>23</sup> G. Leitmann, *The Calculus of Variations and Optimal Control*, Mathematical Concepts and Methods in Science and Engineering, Vol. 24, edited by A. Miele (Plenum Press, New York, 1981).  
<sup>24</sup> G. Knowles, *An Introduction to Applied Optimal Control* (Academic Press, New York, 1981).  
<sup>25</sup> Y. B. Kim, C. F. Hempstead, and A. Strnad, Rev. Mod. Phys. **36**, 43 (1964).  
<sup>26</sup> G. P. Gordeev, L. A. Akselrod, S. L. Ginzburg, V. N. Zabenkin, and I. M. Lazebnik, Phys. Rev. B **55**, 9025 (1997).  
<sup>27</sup> L. M. Fisher, A. V. Kalinov, I. F. Voloshin, I. V. Baltaga, K. V. Il'enko, and V. A. Yampolskiĭ, Sol. State Commun. **97**, 833 (1996).  
<sup>28</sup> L. M. Fisher, K. V. Il'enko, A. V. Kalinov, M. A. R. LeBlanc, F. Pérez-Rodríguez, S. E. Savel'ev, I. F. Voloshin, and V. A. Yampolskiĭ, Phys. Rev. B **61**, 15382 (2000).

FIG. 1. Field and current density penetration profiles for a zero field cooled slab. The dots indicate the initial process in which  $H_z$  was raised to the value  $H_{zS} = 0.6$  at the surface. The successive steps increasing  $H_{yS}$  are labelled from 1 to 5. Continuous lines are used for  $H_z(x)$  and the associated current density  $-J_y(x)$ , while dashed curves represent  $H_y(x)$  and  $J_z(x)$ . Dimensionless units are used as defined in the text.

FIG. 2. Field and current density penetration profiles for a small amplitude cycle in  $H_{yS}$ , successive to the initial magnetization process described in Fig.1. The descending branch curves are labelled 1 to 7 (continuous lines), whereas ascending curves are labelled 8 to 14 (dash-dotted curves). The  $H_z(x)$  and  $-J_y(x)$  profiles nearly repeat values for the descending/ascending processes as one can see in the graph. Some labels have been skipped to avoid confusion.

FIG. 3. Field and current density penetration profiles for an intermediate amplitude cycle in  $H_{yS}$ , successive to the initial magnetization process described in Fig.1. The curves labelled 1 to 6 (continuous lines) stand for the descending process, while the curves 7 to 11 (dash-dotted) stand for the ascending part. The label no.7 in the family of curves  $H_z(x)$  has been avoided for clarity.

FIG. 4. Field and current density penetration profiles corresponding to a high amplitude cycle in  $H_{yS}$ , successive to the initial magnetization process described in Fig.1. Here, we have labelled 1 to 7 the profiles for the initial increase to the high amplitude ( $H_{yS} = 3$ ). The descending branch curves are labelled 8 to 14. In order to avoid confusion, the family of ascending branch curves of the cycle are not displayed.

FIG. 5. Diagram of the square control space  $\Delta$  on purpose for the DCSM oriented according to the local magnetic field. For illustration, we plot the optimal control solution  $\vec{u}$  which maximizes  $\vec{p} \cdot \vec{u}$  in a generic situation. Some specific values  $\vec{p}_1, \vec{p}_2, \vec{p}_3, \dots$  and the corresponding solutions  $\vec{u}_1, \vec{u}_2, \vec{u}_3, \dots$  are also marked. The sequence is extracted from the example depicted in Fig.6.

FIG. 6. Normalized field modulus and angle penetration profiles ( $H(x)/H_S, \alpha(x)/\alpha_S$ ) obtained by the application of our variational principle to the DCSM control space. A field cooled slab was assumed, subjected to further rotation of the surface field. Also depicted are the associated momenta ( $p_h(x), p_\alpha(x)$ ). The points 1 to 5 labelled on the momenta curves correspond to the sequence of control values shown in Fig.5. Following the notation introduced in Ref. 12, we have marked the CT, C and O zones, as well as the penetration points  $x_v$  and  $x_c$ . The distance  $x$  is given in units of the slab half-width  $x_m$ . Contrary to our choice in the rest of figures, in this case  $x = 0$  corresponds to the surface of the slab.

FIG. 7. Evolution of the magnetization components in a simulated crossed field experiment for a zero field cooled superconducting slab. Subsequent to the application of a constant surface field  $H_{zS}$ , the other component  $H_{yS}$  was cycled ( $0 \rightarrow H_m \rightarrow -H_m \rightarrow H_m$ ) for three different values of  $H_m$ . Continuous lines stand for low fields, continuous-dotted for intermediate fields and dashed lines represent the high field cycle.

FIG. 8. First and second magnetization cycles for the intermediate field loop considered in Fig.7.

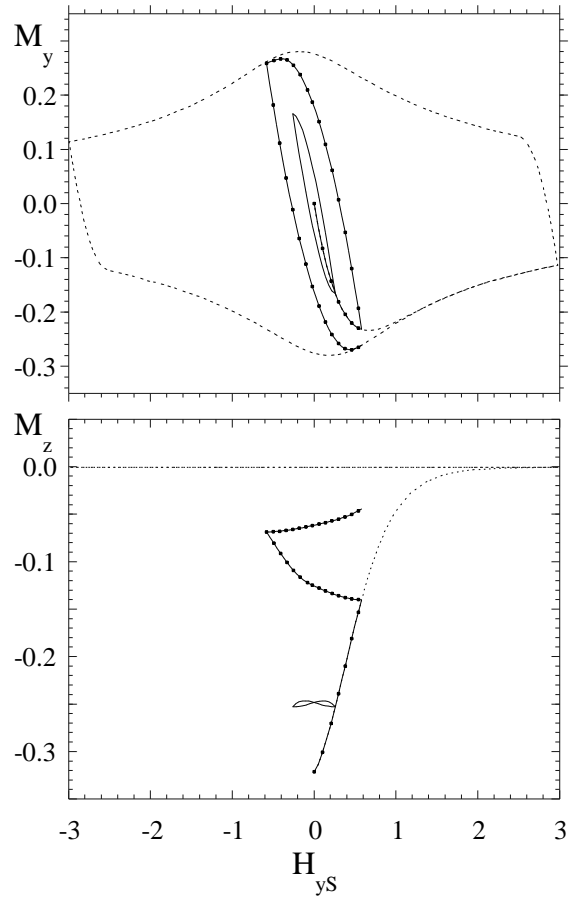
FIG. 9. Dependence of the transverse magnetization  $M_z$  on the first cycle of  $H_{yS}$  ( $0 \rightarrow H_m \rightarrow -H_m \rightarrow H_m$ ) for the para- and diamagnetic initial states in  $H_z(x)$ . The upper panel shows the suppression of  $M_z$  in the paramagnetic case (sequence O'A'B'C') and the lower panel reflects the same phenomenon for the diamagnetic case (sequence OABC). The insets illustrate some selected penetration profiles of  $H_z(x)$ , corresponding to the points labelled on the  $M_z$  curves.

This figure "prb\_vmh\_fig3.jpeg" is available in "jpeg" format from:

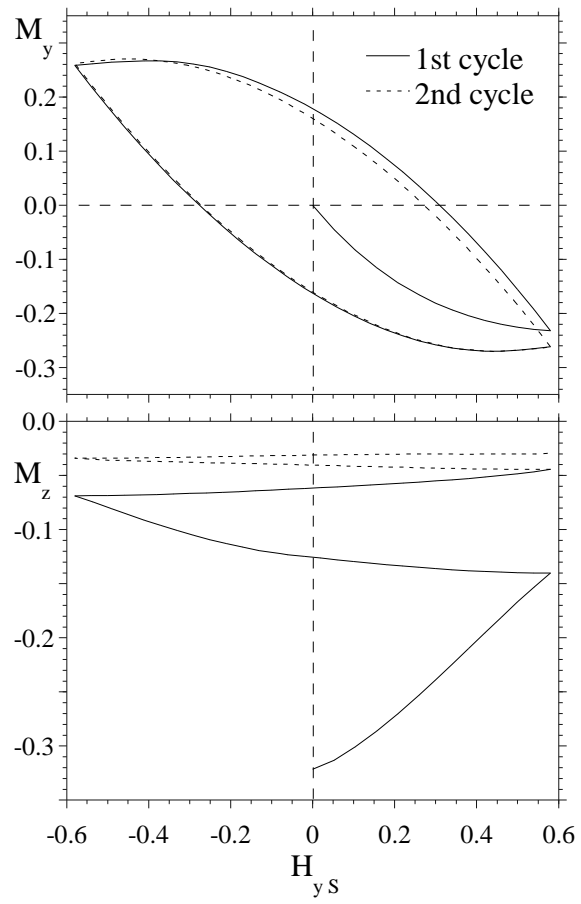
<http://arxiv.org/ps/cond-mat/0112284v1>

This figure "prb\_vmh\_fig4.jpeg" is available in "jpeg" format from:

<http://arxiv.org/ps/cond-mat/0112284v1>



prb\_badia\_fig7



prb\_badia\_fig8

This figure "prb\_vmh\_fig9.jpeg" is available in "jpeg" format from:

<http://arxiv.org/ps/cond-mat/0112284v1>

This figure "prb\_vmh\_fig12.jpeg" is available in "jpeg" format from:

<http://arxiv.org/ps/cond-mat/0112284v1>

This figure "prb\_vmh\_fig56.jpeg" is available in "jpeg" format from:

<http://arxiv.org/ps/cond-mat/0112284v1>